Preprint Title Relationship between morphological and physical properties in nanostructured $CuMnO_2$

Authors Hoa T. Q. Nguyen and Hung V. Tran

Publication Date 09 Okt. 2020

Article Type Full Research Paper

ORCID® iDs Hoa T. Q. Nguyen - https://orcid.org/0000-0002-0955-8241; Hung V. Tran - https://orcid.org/0000-0001-8811-8991

Relationship between morphological and physical properties in nanostructured CuMnO2

Thi Quynh Hoa NGUYEN[1] and Vinh Hung TRAN*[2]

Address: [1]School of Engineering and Technology, Vinh University, 182 Le Duan, Vinh city, Viet nam and [2]Institute of Low Temperature and Structure Research, Polish Academy of Sciences, P.O. Box 1410, 50-422 Wroclaw, Poland

Email: Vinh Hung TRAN - V.H.Tran@intibs.pl

* Corresponding author

Abstract

In this study, crednerite $CuMnO_2$ nanostructures were prepared using a hydrothermal method at 100 °C with different amounts of NaOH mineralizator. Obtained nanostructured crednerite $CuMnO_2$ with monoclinic structure (space group C2/m) exhibits two kinds of morphologies: nanobelts of the length of 1 - 1.5 µm and thickness of 15 -25 nm, and nanoplatets being of 50 - 70 nm in diameter. Comparative studies of the preprepared samples reveal an intimate relationship between morphological and physical properties in nanostructured $CuMnO_2$. A low NaOH concentration favours elongated crystal growth along the c-axis, creating nanobelt-shaped morphology. On the other hand, a strong base solution promotes the formation of nanoplates. Unique morphologies of nanostructured $CuMnO_2$ affect distinct spectroscopic and magnetic properties. The nanobelt-shaped sample is characterized by the Raman active A_{1g} mode at 637 cm^{-1} and a modified Curie-Weiss bahaviour. This phase exhibits two successive magnetic phase transitions: ferromagnetically at 9.2 K and antiferromagnetically at 42 K. Conversely, the nanoplate-shaped sample behaves typically as those reported in the literature, namely, the Raman active A_{1g} mode at 688 cm^{-1} and low-dimensional magnetism with antiferromagnetic ordering below 62 K. The variation in the magnetic properties is presumably associated to the partial oxidation of Cu^{1+} and Mn^{2+}

in the nanoplate-shaped sample compared to the divalent state of Cu^{2+} and trivalent Mn^{3+} ions in the nanobelt-shaped one.

Keywords

nanostructured crednerite, nano-belt, morphology, magnetic properties

Introduction

The mineral crednerite was discovered by Credner [1] and described by Rammensberg [2] to possess chemical formula $3CuO{\cdot}2Mn_2O_3$. However, the proper chemical stoichiometry was determined until a hundred years later by Kondrashev [3], who proposed to be of $CuMnO_2$ and crystal structure to belong to the space group C2/m. A detailed structural study of this compound was stated yet later; and a monoclinic structure was confirmed based on the powder diffraction data [4]. The atomic positions of atoms were resolved based on the single crystal diffraction data, where the Cu atoms occupy the 2d, the Mn atoms locate at the 2a, and the O atoms are distributed at the 4i positions.

In the last few decades, there has been a renewed interest in the research on the $CuMnO_2$ material due to its an exceedingly rich spectrum of potential applications. As a p-type semiconductor [5-7], electrode material [8], $CuMnO_2$ has also been examined regarding photocatalytic activities for hydrogen production or hydrogen storage [9-11], oxygen storage [12,13], energy storage [14,15] as well as in the context of multiferroic peculiarities [16]. Remarkably, by the use of a hydrothermal method, nanoparticles with diameters of 50 -100 nm [6], or nanowires [15], can be obtained. These findings open new routes towards wider possibilities of investigations and applications.

Available information from the literature on synthesises indicates that the $CuMnO_2$ compound can be synthesized via several methods including hydrothermal methods [5,6], ion exchange reactions [10], solid state reactions [13,17,18] and sol - gel techniques [19,20]. The crystal structure of the C2/m space group and lattice parameters of samples from different preparations are essentially consistent with each other experiment, but their physical properties differ dramatically. For instance, direct optical gap was found to have various values from 1.4 eV [5] through 2.6 - 3.5 eV [21] to

4.6 eV [18]. Remarkably, studies of magnetic properties reported for $CuMnO_2$ pointed to a serious discrepancy too. Mostly, an antiferromagnetic (AF) phase transition below about 65 K was established for bulk compounds [22-25]. However, completed incompatibilities were observed for nano-sized materials; AF order seems to take place below 42 K in nanoparticles with the sizes of 50-100 nm [16] and nonmagnetic for particles with a diameter of about 300 nm [26]. It is possible that manifold physical properties of $CuMnO_2$ are caused by multiple mechanisms. The miscellaneous morphologies of the nano-sized particles and bulk crystal structured materials of $CuMnO_2$ should be the first factor relevant. At the nanoscale, besides the exchange interactions between d-electron magnetic moments, the dimensionality and dipole magnetic interactions are substantial components for the formation of a ground state. The most natural method of preparing different morphologies of nanoparticles is that which can modify condition of reaction, e.g., by varying factors such as precursor solution and its concentration, reaction temperature, reaction time and pH value of the solvents. A successful synthesis upon changes of reaction condition has been documented for delafossite $CuGaO_2$ [27] or for crednerite $CuMnO_2$ [15,28]. Fu et al. [15] showed that the valence states of samples consisting of Cu^{1+}, Cu^{2+}, Mn^{2+} and Mn^{3+} are possibly adjusted varying reaction temperatures. As a result, morphologies of the $CuMnO_2$ nanoparticles are changed in a consequence triangular sheets - nanowires - hexagonal prisms - octahedrons with creasing temperature. Conversely, Xiong et al. [28] used diverse amounts of NaOH and reaction components, and applied several temperatures. The authors were able to obtaine single-crystalline $CuMnO_2$ nanoparticles of diameters 100 - 150 nm for a large amount of NaOH or at temperatures higher than 80 °C. Unfortunately, an attempt to synthesize a pure sample was performed with a low NaOH concentration and at 80 °C but no successful achievements were scored. Thus, understanding the mechanisms by which the morphology and size of the crystals can be effectively controlled by pH values remain an ongoing challenge of material research. In particular, the impact of morphologies of nanostructured samples upon magnetic properties is still an open issue. In this article, we report the synthesis of nanostructured $CuMnO_2$ samples using a hydrothermal method employed in previous studies, e.g. as described by Krause and Gawryck many years ago [29], and reported in the

literature for synthesis of delafossites [15,28,30,31]. Because, the reaction between (OH) and Mn^+ plays an important role in the formation of MnO_6 octahedron, we use several amounts of NaOH mineralizator, i.e., 1g, 2g and 3g per 35 ml of solution, to turn the reaction rates and the degree of nucleation. Then, we determine morphologies, chemical compositions and crystallographic data of the obtained samples along with their spectroscopic (Raman and UV-VIS) and magnetic (dc-magnetization, ac-susceptibility) properties.

Experimental details

All chemicals used in our experiments were of analytical grade and have been used as received without any additional purification. In our synthesis, we used 7.5 mmol of $Cu(NO_3)_2{\cdot}3H_2O$ and 7.5 mmol of $MnCl_2{\cdot}4H_2O$, which were dissolved in 35 ml of deionized water, then a suitable amount of NaOH as a mineralizator was added to the above solution. The reaction mixture was sonicated for 5 min and followed by stirring for 10 minutes to ensure homogeneity of the blend. The growth solution was transferred into a 50 ml teflon-lined stainless steel. The reaction was maintained at temperature of 100 °C for 24 h. After the reaction, the autoclave was cooled down to room temperature naturally. The precipitate was collected via centrifugation, washed with deionized water and absolute alcohol in sequence several times, and stored in absolute alcohol solution. Before the physical properties measurements, samples were dried in air. In order to study the possible influence of pH on the chemical process in $CuMnO_2$ synthesis, different amounts of NaOH, i.e., 1.0, 2.0 and 3.0g, have been added in consecutive synthesises. Following the above procedures, we obtained three different nanostructured $CuMnO_2$ samples. Hereafter, the samples are denoted as nr 1, nr 2 and nr 3, respectively. Our synthesis procedure differs little from that used by Xiong et al. [28] by used NaOH amounts and reaction temperature. The obtained $CuMnO_2$ nanostructures have been characterized as regards morphologies, composition and crystal structures, including lattice parameters and nanoparticle sizes. For these purposes, we used a Schottky field-emission scanning electron microscopy (FESEM) system (JEOL JSM-7600F, operated at 10.0 kV), which is equipped with energy-dispersive X-ray spectroscopy (EDX) and a X'Pert PRO diffractometer with

monochromatic CuK_α radiation operated at an accelerating voltage of 40 keV and 30 mA. Measured X-ray powder diffraction spectra in the 2θ range of 10 - 80 deg, were analysed by means of the Rietveld refinement method using the FullProf program [32]. Further experiments have been done aiming to determine the vibrational modes of molecules and atoms, as well as optical absorption by nanostructured particles. In this case, the Raman spectra were collected using a LabRAM HR800 (Horiba) with a 632.8 nm excitation laser at a resolution of 1.0 cm^{-1}. Whereas the UV-visible reflectance mode was gauged utilizing an Agilent 8453 UV-visible spectrophotometer. Finally, measurements of magnetic quantities such as ac-, dc-magnetic susceptibility and magnetization were performed in the temperature range between 2 and 300 K and in magnetic fields up to 7 T with the aid of Quantum Design MPMS-XL7.

Results and Discussion

Morphological, chemical and crystallographic analysis

In Fig. 1, we present the SEM and EDX spectra for nano-sized $CuMnO_2$ samples, obtained by the adding three different amounts of NaOH to the reaction solution. By comparing the observed SEM images, we recognize that the pH has considerable effect on morphologies. The synthesis with 1g of NaOH results in $CuMnO_2$ nano-belts of the length of about 1 - 1.5 µm, width of 50 - 80 nm and thickness of 15 - 25 nm. To the best of our knowledge, crednerite $CuMnO_2$ nanobelts were successfully synthesized for the first time. As distinguished from the 1g NaOH preparation, the nanoparticles from samples conceived with using 2 or 3g exhibit morphologies of nanoplate-like geometry, being of 50 - 70 nm in diameter. Between these latter samples, there exists a difference in morphologies associated with the presence of an agglomeration of nanoparticles in sample nr 2 but well separately nanoparticles in sample nr 3.

The elemental analyses of $CuMnO_2$ by EDX are shown in the right panels of Fig. 1. The present peaks affirm the presence of Cu, Mn and O elements. However, the atom ratio of Cu:Mn:O does not match the ideal 1:1:2 ratio. Taking into consideration of the fact that the at.% of O is less than 50 and the presence of a small quantity of at.% Cl, we anticipate that the Cl atoms would

share some places with the O atoms in the 4i position. Moreover, we discern that the at.% of Cu is larger than that of Mn, implying that the Cu atoms possibly occupy in part the 4a position of Mn. Based on this consideration, we would propose the chemical stoichiometry of our samples like that $Cu_xMn_{1-x}O_{2-y}Cl_y$ with x ~ 0.15 and y ~ 0.05. We admit however that proper stoichiometry of the prepared samples should be determined with more sophisticated methods than these used in this work.

The X-ray powder diffraction patterns of the studied samples are shown in Fig. 2. Since the compound $CuMnO_2$ has previously been reported to crystallize in a monoclinic structure with space group C2/m [33], and possible in delafossite-type hexagonal (trigonal) with space group P63/mmc (R-3m) [34], we have analysed the experimental data with respect to these structure types. In turn, our x-ray patterns support neither hexagonal nor trigonal structure but well conform to the monoclinic one. We must emphasise that any foreign impurity is not observed, obviously, within the instrument detection limit. An important finding is that the strong peak at 2θ =15.8 deg. for hkl = 001 and 2θ =31.5 deg. for hkl = 002 are clearly visible in the X-ray pattern for sample nr 1, indicating the preferred orientation of the grains along the c-axis. The broadness of the peaks in all spectra are due to weakly crystalline nature of the product since in fact are of nanoparticles. The average crystallite sizes of the samples were estimated with the Si(111) single crystal standard and using Scherrer's equation: $L = K\lambda/(\beta cos(\theta))$; where L is the mean size of the ordered grains, K is a shape factor constant assumed to be 0.9, λ is the X-ray wavelength and β is peak width at FWHM of the Bragg angle θ. Our analysis yielded sizes of grains from 17 to 65 nm for sample nr 1, from 16 to 30 nm for nr 2, and from 15 to 24 nm for nr 3, being consistent with the SEM data.

The refinements yield good agreement between theoretical profile (solid line) and measured one (open symbols) (see Fig.2). The refined convergence parameters were found as follow: R_p = 2.7, R_{wp} = 4.2 and χ^2 = 4.5.1 for nr 1, R_p = 2.0, R_{wp} = 2.4 and χ^2 = 2.0 for nr 2, and R_p = 1.9, R_{wp} = 2.6 and χ^2 = 2.0 for nr 3. Given in TABLE 1 our lattice parameters correspond well with published data [16,18,33,35]. We found that the smallest amount of NaOH causes the drop of both parameters a and c of the unit cell. Therefore, it is interesting to recall that the a parameter is related to the

geometry of MnO_6 octahedron and the c is intimated with the O-Cu-O length. From the presented here results, it is clear that different NaOH concentrations in the synthesis effect on the distinct stoichiometry, crystallographic parameters of the prepared product and obviously on its morphology.

Spectroscopic properties

In Fig. 3 we present the frequency dependence of the Raman shift in the studied samples. As reported in literature, the delafossites $CuMnO_2$ (M = Cr, Fe) exhibit two Raman active modes, assigned to the modes A_{1g} and E_g. The active mode A_{1g} appears around 700 cm^{-1}, corresponding to the vibration of O-Cu-O linkage along the c-axis while the two weak Raman active E_g modes located between 350 cm^{-1} and 420 cm^{-1} resulted from the vibration of MO_6 octahedra along the a-axis [21,36]. Spectral data of our nanostructured $CuMnO_2$ samples exhibit strong peak at 637 cm^{-1} in the sample nr 1 and 688 cm^{-1} in the samples 2 and 3, which are certainly attributed to the A_{1g} wagging vibrational modes. In the lower wave numbers, there are very weak anomalies at 305 and 382 cm^{-1}, and they presumably represent the E_g stretching modes. In addition to these peaks, we detect pronounced singularity around 570 cm^{-1} in the samples nr 2 and nr 3. This mode may be interpreted as due to the Mn-O bending, because this singularity resembles the vibration of the Co-O linkage in $LiCoO_2$ [37]. It is worthwhile to note that the position of main Raman peak of the sample nr 1 is moved down by 50 cm^{-1} compared to those of the samples nr 2 and 3. Moreover, the linewidth of this peak is broader. The distinct behaviour of the sample nr 1 may be associated with the deduced lattice parameters and sizes of nanoparticles, as were considered above.

The spectral characteristics of the absorption coefficient α of the nanostructured $CuMnO_2$ films prepared using three different amounts of NaOH are presented in Fig. 4. The pronounced absorption peak at 287 nm and a broadened knee in the range 480 - 580 nm are observed in our nanostructured samples. The presence of these peaks points to the d - d transitions in electronic band structure. Following the interpretation given by Hiraga et al. [38], the first absorption peak is an excitonic absorption combined with transition from the valence band of O 2p to the conduction band of Cu 3d4s states, and the extended knee in the absorption spectrum may be contributed to the

electron excitation from valence band to Mn t_{2g} orbitals. The optical transition in the absorption spectrum (Fig. 4) is used to determine the energy gaps through the Tauc relation [39]:

$$h\nu^{1/n} = A(h\nu - E_g) \tag{1}$$

where A is a constant, E_g is the optical bandgap of a given material, and n is equal to 1/2, 2 or 3/2 respectively for indirect, direct or direct forbiden transitions. We plot in Fig. 5 the photon energy dependence of experimental ($h\nu^{1/n}$) data for n = 2 in the left scale and n = 1/2 in the right scale. Fitting of eq. 1 to the data yields direct gaps in the range 3.17 - 3.74 eV and indirect gaps of 0.98 - 2.29 eV. Experimental energy gap E_g values found in our samples are smaller than these reported by Shukla et al. with E_g of 4.6 eV and 4.90 eV, respectively [18]. Smaller values of optical gaps in our samples suggest a shift of the Fermi level down towards the valence band edge.

Magnetic properties

The influence of pH on the chemical process in the synthesis and in a consequence on the physical properties of nanostructured $CuMnO_2$ samples is clearly established from the study of magnetic behaviour present in Figs 6 - 10. An analysis of the inverse magnetic susceptibility, χ^{-1}(T) of sample nr 1 determined in a field of 0.15 T versus temperature (Fig. 6) reveals that the magnetic susceptibility above 100 K fulfils a modified Curie-Weiss dependence:

$$\chi(T) = \frac{C}{T - \theta_p} + \chi_0 \tag{2}$$

with the paramagnetic Curie temperature of θ_p = - 89(3) K, χ_0 = 6.5×10^{-4} emu/mol and Curie constant per each transition metal (TM) C = 0.616 emuK/mol$_{TM}$. The latter value corresponds to an average value of the effective moment μ_{eff} = 2.22(0.03) μ_B per each Cu and Mn magnetic ion, and quite agrees with the theoretical value for $Cu^{2+}$of 1.73 μ_B and for low-spin Mn^{3+} of 2.83 μ_B: $\mu_{eff} = \sqrt{0.5 * \mu^2_{Cu^{2+}} + 0.5 * \mu^2_{Mn^{2+}}} = \sqrt{0.5 * 1.73^2 + 0.5 * 2.83^2} = 2.34\ \mu_B$. Clearly, our data differ from those reported by Trari et al., who observed high-spin configuration for Mn^{2+} in $CuMnO_2$

samples obtained via a solid state reaction [22]. Moreover, our experiments lead also to different results than reported in the literature as regards to the magnetic phase transitions. On the one hand, we detect as many as two transitions at T_C = 9.2 K and T_N = 42 K in our sample (see inset). On the other hand, previous researchers reported only one antiferromagnetic phase transition at around 65 K [22-25] for bulk or only one transition at 42 K for a nano-sized $CuMnO_2$ material [16].

To shed more lights on complex phase transitions, we conducted additional measurements of magnetic quantities at low temperatures and in magnetic dc-fields and ac-frequencies. The magnetization at 2 and 25 K (see Fig. 7 a) divulges a magnetic hysteresis below T_C and lacking hysteresis below T_N. Further ample evidence for ferromagnetic characteristics is illustrated in Fig. 7 b), where the increase of applied dc-magnetic fields raises the T_C values. The anomalies in the real and imaginary components of the ac-susceptibility (Fig. 8) attach to a ferromagnetic support for this sample below T_C. We may add that the ac-susceptibility measurements do not detect loss peak in the imaginary component at T_N (not shown here), thus the transition at T_N is most probably antiferromagnetic.

Fig. 9 displays the magnetic behaviour of the sample nr 2. Apparently, the magnetic measurements in fields up to 1 T uncover two magnetic phase transitions at 62 K denoted as $T_N(1)$ and at 40 K denoted as $T_N(2)$. The data collected in several low magnetic fields reveal a broad maximum, which a little moves to lower temperatures with increasing applied magnetic fields, corroborating antiferromagnetic character of the transition at $T_N(2)$. It is also found that temperature dependence of the inverse magnetic susceptibility in the paramagnetic regime exhibits unambiguous properties different than that of the sample nr 1. First, the description of $\chi(T)$ in the temperature range 200 - 300 K with a Curie - Weiss law yields the average effective moment 4.23 μ_B per transition metal ion and Curie-Weiss temperature -775 K. A large μ_{eff} value refers the high-spin state of the Mn^{2+} and nonmagnetic state of Cu^{+}. Second, the broad maximum in the $\chi(T)$ curve around 150 K may reflect the low-dimensional nature of the antiferromagnetic interactions between the Mn^{2+} ions. Our result supports consideration of Jia et al. [40], who showed that the magnetic coupling between Mn layers is weak, intimating a 2D characteristic. Although $CuMnO_3$, owing to kagomé lattice of mo-

ment arrangements, has been recognized as a frustrated system, the exchange constant between the nearest neighbours J_1 was found to be much larger than those between next-nearest neighbours J_2 and next-next-nearest neighbours J_3 [40]. So, in the first approximation, one applies the Heisenberg model for chain Mn-based systems with S = 5/2, e.g., on $CsMnCl_3$ [41], $[(CH_3)_4N][MnCl_3]$ [42] and $CsMnBr_3$ [43]. For the sample studied here, we applied the model developed by Fisher [44]:

$$\chi(T) = \frac{N_A g^2 S(S+1)\mu_B^2}{k_B T} \frac{1+u}{1-u} + \chi_0 \tag{3}$$

where $u = Coth[[2JS(S+1)/k_BT] - k_BT/[2JS(S+1)]]$, N_A is the Avogadro number, k_B is the Boltzmann constant, g is Land´e factor and J is the antiferromagnetic exchange constant coupling between nearest neighbors and S = 5/2 of Mn^{2+} ions. The theoretical curve shown in Fig. 9 as a dotted line, was obtained for g = 2 and J/k_B = - 16.8 K and χ_0 = 0.3×10^{-4} emu/mol. The well agreement between the theoretical model and experimental data suggests the fulfil of Heisenberg model in magnetic susceptibility properties of $CuMnO_2$ nr 2.

The magnetic properties of $CuMnO_2$ nr 3 are presented in Fig. 10. Basically, the high-temperature susceptibility does not differ considerably from that of the sample nr 2. From the Curie-Weiss fitting, we obtain μ_{eff} = 4.08 μ_B per transition metal ion and Curie-Weiss temperature - 719 K. A broad maximum in $\chi(T)$ around 150 K is again observed and it is a hallmark of low-dimensional magnetism. The theoretical curve of eq. 3 is seen to be in well agreement with the experimental data, and we derive J/k_B = -17.2 K and and χ_0= 0.32×10^{-4} emu/mol (see dotted line).

Around 42 K, there appears an anomaly denoted as T^*, below which the susceptibility rapidly rises with further decreasing temperature. One suspects that some ferromagnetic interactions between next-next-nearest neighbours, as were determined by Jia et al. [40], start to play a role. However, in samples 2 and 3, large values of paramagnetic Curie temperature θ_p and also Heisenberg exchange interaction coupling J indicate a net antiferromagnetic interaction between the Mn^{2+} magnetic moments. As could be expected, magnetization at 2 K does not show hysteresis (see inset of Fig. 10), and a ferromagnetic ground state in samples 2 and 3 can be excluded.

Summary

Table 1: A comparison of the EDX, crystallographic, Raman, UV-VIS and magnetic data of three nanostructured $CuMnO_2$ samples obtained via adding 1g, 2g and 3g NaOH to reaction solution.

Quantities	1 g NaOH	2g NaOH	3g NaOH
O (at. %)	42.4	45.0	45.0
Cu (at. %)	31.0	29.8	31.2
Mn (at. %)	24.3	24.3	23.8
a (nm)	0.55034	0.55865	0.55737
b (nm)	0.28931	0.28855	0.28852
c (nm)	0.58793	0.58986	0.59058
Raman peak (cm^{-1})	637	688	688
Direct gaps (eV)	3.52, 5.74	3.41, 3.72	3.17, 3.68
Indirect gaps (eV)	1.54, 1.91	1.45, 2.29	0.98, 1.17
Ordering temp.	T_C = 9.2 K, T_N = 42 K	$T_N(2)$ = 40 K, $T_N(1)$ = 62 K	T^* = 42 K
Mag. characteristics	MCW, 3D	CW, LD	CW, LD
μ_{eff} (μ_B)	2.22	4.23	4.08
θ_p (K)	-89	-775	-719
J/k_B (K)	-	-16.8	-17.2

The nanostructured $CuMnO_2$ samples were synthesized by low-temperature hydrothermal method. The obtained samples were characterized in terms of morphologies, chemical compositions and crystallography along with the spectroscopic (Raman and UV-VIS) and magnetic (dc-magnetization, ac-susceptibility) properties. The physical parameters resulted from the measurements are gathered in TABLE 1. Our experiments indicate that both morphological and preferred crystal growth of nanostructured $CuMnO_2$ and then their physical properties can be tuned utilizing suitable amounts of NaOH mineralizator in the growth solution. The SEM and Xray powder diffraction experiments divulge that a pure $CuMnO_2$ phase of monoclinic structure can been prepared in the form of nano-belts with lengths up to 1.5 µm or nanoplates possessing 50 - 70 nm in diameter. The physical properties measurements imply distinct behaviour amongst these samples. The $CuMnO_2$ nano-belts exhibits Raman peak at a lower Raman number compared to that of the nanoplates. Regarding to the magnetic characteristics, the nanobelt samples have shown to be undergone into two successive magnetic phase transitions and at lower temperatures. The most important finding in this work is that utilizing different amounts of NaOH mineralizator influences the morphologies and preferred crystal growth, which next affect the physical properties of the cred-

nerite $CuMnO_2$. The variation in the magnetic properties would be ascribed to the partial oxidation of Cu^{1+} and Mn^{3+} in the nanoplate-shaped samples compared to Cu^{2+} and Mn^{2+} in the nanobelt-shaped one. Admittedly, further investigations using spectroscopic techniques such as XAS and XPS is highly desired to determine precisely valences of atoms involved in the materials. Finally, we are believed that our results extend our fundamental understanding of atomic processes, which underlay the morphological modulations of the $CuMnO_2$ materials and their physical properties, thus creating a new path to obtain selected nanoparticles with desirable properties.

References

1. H. Credner, Uber das vorkommen von vanadinsaurem kupier-oyxd und kufer-manganerz bei friedrichroda im thuringer wald, Neues Jahrbuch 295 1847A (1847) 1.

2. C. Rammelsberg, Uber das mangankupfererz von friedrichroda; zusatz zu der vorhergehenden abhandlung, Ann. Phys. - Leipzig 74 (1848) 559 - 561.

3. I. D. Kondrashev, The crystal structure and composition of crednerite, $CuMnO_2$, Sov. Phys. Crystallogr. 3 (1959) 703 - 706.

4. C. Gaudefroy, J. Dietrich, F. Permingeat, P. Picot, La crednerite. sa composition chimique et sa signification gntique, Bull. Soc. Franc. Miner. Crist. 89 (1996) 80 - 88.

5. Q. ul Ain Javed, F. Wang, A. M. Toufiq, M. Y. Rafique, H. Mahmood, Conspicuous reversible phase transformation of novel $Cu_{1.4}Mn_{1.6}O_4$ square nanosheets synthesized by auto-thermal process exhibiting intriguing optical and magnetic properties, Mater. Lett. 99 (2013) 134 - 137. doi:https://doi.org/10.1016/j.matlet.2013.02.081.

6. Q. Zhang, D. Xiong, H. Li, D. Xia, H. Tao, X. Zhao, A facile hydrothermal route to synthesize delafossite $CuMnO_2$ nanocrystals, J. Mater. Sci.: Mater. Electron. 26 (2015) 10159 - 10163.

7. N. Benreguia, A. Barnabé, M. Trari, Preparation and characterization of the semiconductor $CuMnO_2$ by sol-gel route, Mater. Sci. Semicond Process 56 (2016) 14 - 19. doi:https://doi.org/10.1016/j.mssp.2016.07.012.

8. S. S. Siwal, Q. Zhang, C. Sun, V. K. Thakur, Graphitic carbon nitride doped copper - manganese alloy as high -performance electrode material insupercapacitor for energy storage, Nanomaterials 10 (1) (2020) 2.

9. P. Porta, G. Moretti, M. Musicanti, A. Nardella, Copper-manganese mixed oxides: formation, characterization and reactivity under different conditions, Solid State Ionics 63-65 (1993) 257 - 267. doi:https://doi.org/10.1016/0167-2738(93)90114-I.

10. Y. Bessekhouad, M. Trari, J. Doumerc, $CuMnO_2$, a novel hydrogen photoevolution catalyst, Int. J. Hydrogen Energ 28 (1) (2003) 43 - 48. doi: https://doi.org/10.1016/S0360-3199(02)00023-X.

11. S. A. Abdel-Hameed, F. H.Margha, A. A. El-Meligi, Investigating hydrogen storage behavior of $CuMnO_2$ glass-ceramic material, Int. J. Energy Res. 38 (4) (2014) 459 - 465. doi:10.1002/er.3102.

12. S. Kato, R. Fujimaki, M. Ogasawara, T. Wakabayashi, Y. Nakahara, S. Nakata, Oxygen storage capacity of $CuMO_2$ (M=Al, Fe, Mn, Ga) with a delafossite-type structure, Appl. Catal. B-Environ. 89 (1) (2009) 183 - 188. doi:https://doi.org/10.1016/j.apcatb.2008.11.033.

13. X. Huang, C. Ni, G. Zhao, J. T. S. Irvine, Oxygen storage capacity and thermal stability of the $CuMnO_2$ - CeO_2 composite system, J. Mater. Chem. A 3 (2015) 12958 - 12964. doi:10.1039/C5TA01361E.

14. L. Wang, M. Arif, G. Duan, S. Chen, X. Liu, A high performance quasi-solid-state supercapacitor based on $CuMnO_2$ nanoparticles, J. Power Sources 355 (2017) 53 - 61. doi:https://doi.org/10.1016/j.jpowsour.2017. 04.054.

15. S. Fu, L. Li, Y. Jing, Y. Zhang, X. Wang, S. Fang, J. Wang, G. Li, Crystal growth of bimetallic oxides $CuMnO_2$ with tailored valence states for optimum electrochemical energy storage, Cryst. Growth Des. 18 (10) (2018) 6107 - 6116. doi:10.1021/acs.cgd.8b00988.

16. A. Kurokawa, T. Yanoh, S. Yano, Y. Ichiyanagi, Preparation and magnetic properties of multiferroic $CuMnO_2$ nanoparticles, J. Nanosci. 14 (3) (2014) 2553 - 2556.

17. B. Bellal, B. Hadjarab, N. Benreguia, Y. Bessekhouad, M. Trari, Photoelectrochemical characterization of the synthetic crednerite $CuMnO_2$, J. Appl. Electrochem. 41 (2011) 867 - 872.

18. K. K. Shukla, P. Shahi, G. S., A. Kumar, A. K. Ghosh, R. Singh, N. Sharma, A. Das, A. K. Sinha, A. G. Joshi, A. K. Nigam, S. Chatterjee, Magnetic and optical properties of fe doped crednerite $CuMnO_2$, RSC Adv. 5 (2015) 83504 - 83511. doi:10.1039/C5RA13305J.

19. H.-Y. Chen, D.-J. Hsu, Characterization of crednerite-$Cu_{1.1}Mn_{0.9}O_2$ films prepared using solgel processing, Appl. Surf. Sci. 290 (2014) 161 - 166. doi:https://doi.org/10.1016/j.apsusc.2013.11.021.

20. H.-Y. Chen, D.-J. Hsu, X-ray photoelectron spectroscopy studies the cation valencies and distributions in crednerite-$Cu_{1.1}Mn_{0.9}O_2$ thin films, J. Alloys and Comp. 598 (2014) 23 - 26. doi:https://doi.org/10.1016/j.jallcom.2014.02.018.

21. H.-Y. Chen, Y.-C. Lin, J.-S. Lee, Crednerite-$CuMnO_2$ thin films prepared using atmospheric pressure plasma annealing, Appl. Surf. Sci. 338 (2015) 113 - 119. doi:https://doi.org/10.1016/j.apsusc.2015.02.112.

22. M. Trari, J. Topfer, P. Dordor, J. Grenier, M. Pouchard, J. Doumerc, Preparation and physical properties of the solid solutions $Cu_{1+x}Mn_{1-x}O_2$ ($0 \leq x \leq 0.2$), J. Solid State Chem. 178 (9) (2005) 2751 - 2758. doi.org/10.1016/j.jssc.2005.06.009.

23. F. Damay, M. Poienar, C. Martin, A. Maignan, J. Rodriguez-Carvajal, G. André, J. P. Doumerc, Spin-lattice coupling induced phase transition in the s = 2 frustrated antiferromagnet $CuMnO_2$, Phys. Rev. B 80 (2009) 094410. doi:10.1103/PhysRevB.80.094410.

24. C. Vecchini, M. Poienar, F. Damay, O. Adamopoulos, A. Daoud-Aladine, A. Lappas, J. M. Perez-Mato, L. C. Chapon, C. Martin, Magnetoelastic coupling in the frustrated antiferromagnetic triangular lattice $CuMnO_2$, Phys. Rev. B 82 (2010) 094404. doi:10.1103/PhysRevB.82.094404.

25. N. Terada, Y. Tsuchiya, H. Kitazawa, T. Osakabe, N. Metoki, N. Igawa, K. Ohoyama, Magnetic correlations and the influence of atomic disorder in frustrated isosceles triangular lattice antiferromagnet $CuMnO_2$, Phys. Rev. B 84 (2011) 064432. doi:10.1103/PhysRevB.84.064432.

26. M. Poienar, P. Sfirloaga, C. Martin, D. Ursu, P. Vlazan, Hydrothermal synthesis of crednerite $CuMn_{1-x}M_xO_2$ (M = Mg, Al; x= 0- 0.08): structural characterisation and magnetic properties, J. Mater. Sci. 53 (2018) 2389 - 2395. doi:doi.org/10.1007/s10853-017-1696-z.

27. M. Yu, T. I. Draskovic, Y. Wu, Understanding the crystallization mechanism of delafossite cugao2 for controlled hydrothermal synthesis of nanopar-ticles and nanoplates, Inorg. Chem. 53 (11) (2014) 5845 - 5851, doi:10.1021/ic500747x.

28. D. Xiong, Q. Zhang, Z. Du, S. K. Verma, H. Li, X. Zhao, Low temperature hydrothermal synthesis mechanism and thermal stability of p-type $CuMnO_2$ nanocrystals, New J. Chem. 40 (2016) 6498 - 6504. doi.org/10.1039/C6NJ00253F

29. A. Krause, S. Gawryck, Amorphe und kristallisierte oxydhydrate undoxyde. xliv. die umwandlung des rntgenographisch amorphen eisen iii- hydroxyds in -Fe_2O_3, Z. Anorg. Allg. Chem. 238 (1938) 406 412. doi:10.1002/zaac.19382380409.

30. R. D. Shannon, D. B. Rogers, C. T. Prewitt, Chemistry of noble metaloxides. i. syntheses and properties of ABO_2 delafossite compounds, Inorg. Chem. 10 (1971) 713 - 718. doi:10.1021/ic50098a011.

31. W. C. Sheets, E. Mugnier, A. Barnabé, T. J. Marks, K. R. Poeppelmeier, Hydrothermal synthesis of delafossite-type oxides, Chem. Mater. 18 (2006) 7 - 20. doi:10.1021/cm051791c.

32. T. Roisnel, J. Rodriguez-Carvajal, Winplotr: a windows tool for powder diffraction patterns analysis, Materials Science Forum, Proceedings of the Seventh European Powder Diffraction Conference (EPDIC 7), Ed. R. Delhez and E.J. Mittenmeijer (2000) 118 - 123.

33. J. Topfer, M. Trari, P. Gravereau, J. P. Chaminade, J. P. Doumerc, Crystal growth and reinvestigation of the crystal structure of crednerite, $CuMnO_2$, Z. Krist-Cryst. Mater 210 (3) (1995) 184 - 187.

34. F. C. M. Driessens, G. D. Rieck, Phase equilibria in the system $CuMnO_2$, Z. Anorg. Allg. Chem. 351 (1967) 48 - 62. doi:10.1002/zaac.19673510108.

35. A. A. G. Santiago, R. L. Tranquilin, M. C. Oliveira, R. A. P. Ribeiro,S. R. de Lazaro, M. A. Correa, F. Bohn, E. Longo, F. V. Motta, M. R. D.Bomio, Disclosing the structural, electronic, magnetic, and morphological properties of $CuMnO_2$: A unified experimental and theoretical approach, J. Phys. Chem. C 124 (9) (2020) 5378 - 5388. doi:10.1021/acs.jpcc.0c00198.

36. O. Aktas, K. D. Truong, T. Otani, G. Balakrishnan, M. J. Clouter, T. Kimura, G. Quirion, Raman scattering study of delafossite magnetoelectric multiferroic compounds: $CuFeO_2$ and $CuCrO_2$, J. Phys.: Conden. matt. 24 (3) (2011) 036003. doi:10.1088/0953-8984/24/3/036003.

37. R. Baddour-Hadjean, J.-P. Pereira-Ramos, Raman microspectrometry applied to the study of electrode materials for lithium batteries, Chem. Rev. 425 110 (3) (2010) 1278 - 1319. doi:10.1021/cr800344k.

38. H. Hiraga, T. Fukumura, A. Ohtomo, T. Makino, A. Ohkubo, H. Kimura, M. Kawasaki, Optical and magnetic properties of $CuMnO_2$ epitaxial thin films with a delafossite-derivative structure, Appl. Phys. Lett. 95 (3) (2009) 032109. doi:10.1063/1.3186790.

39. J. Tauc, Optical properties and electronic structure of amorphous Ge and Si, Mater. Res. Bull. 3 (1) (1968) 37 - 46. doi:https://doi.org/10.1016/0025-5408(68)90023-8.

40. T. Jia, G. Zhang, X. Zhang, Y. Guo, Z. Zeng and H. Q. Lin J. Appl. Phys. 109 (2011) 07E102 ; https://doi.org/10.1063/1.3536533.

41. T. Smith, S. A. Friedberg, Linear chain antiferromagnetism in $CsMnCl_3 \cdot 2H_2O$, Phys. Rev. 176 (1968) 660 - 665. DOI:https://doi.org/10.1103/PhysRev.176.660.

42. R. Dingle, M. E. Lines, S. L. Holt, Linear-chain antiferromagnetism in $[(CH_3)_4n]$ $[MnCl_3]$, Phys. Rev. 187 (1969) 643 - 648. doi:10.1103/PhysRev.187.643.

43. W. J. Fitzgerald, D. Visser, K. R. A. Ziebeck, One-dimensional magneticcorrelations in the antiferromagnet $CsMnBr_3$, J. Phys. C: Solid State Phys. 15 (4) (1982) 795 - 799. doi:10.1088/0022-3719/15/4/025.

44. M. E. Fisher, Magnetism in one-dimensional systemsthe heisenberg model for infinite spin, Am. J. Phys. 32 (5) (1964) 343 - 346. doi:10.1119/1.1970340.

Fig. 8

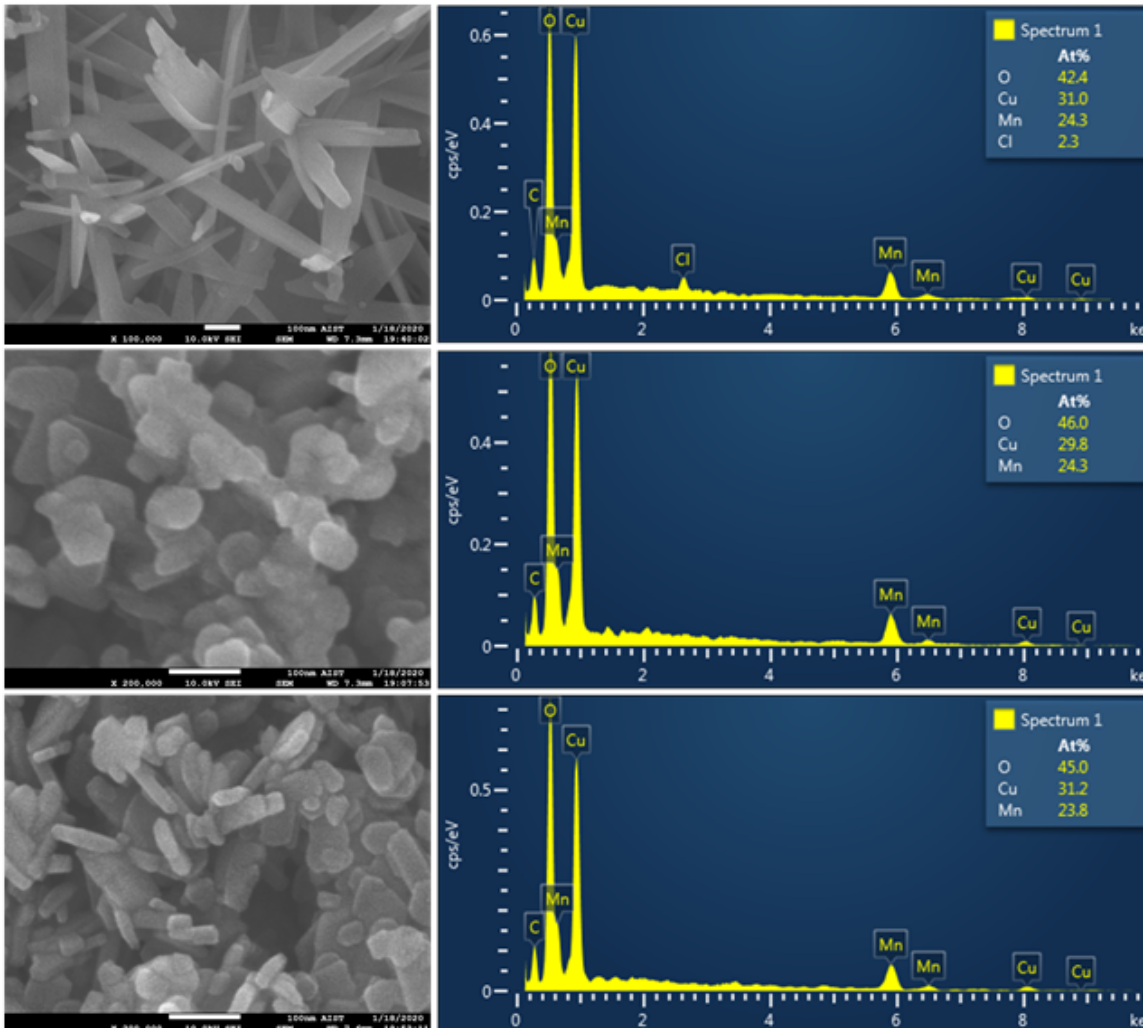

Figure 1: SEM image (Left side) and corresponding EDX spectrum (Right side) of the $CuMnO_2$ nanostructures grown using 1g, 2g and 3g NaOH per 35 ml of reaction solution, shown in the top, middle and bottom panel, respectively

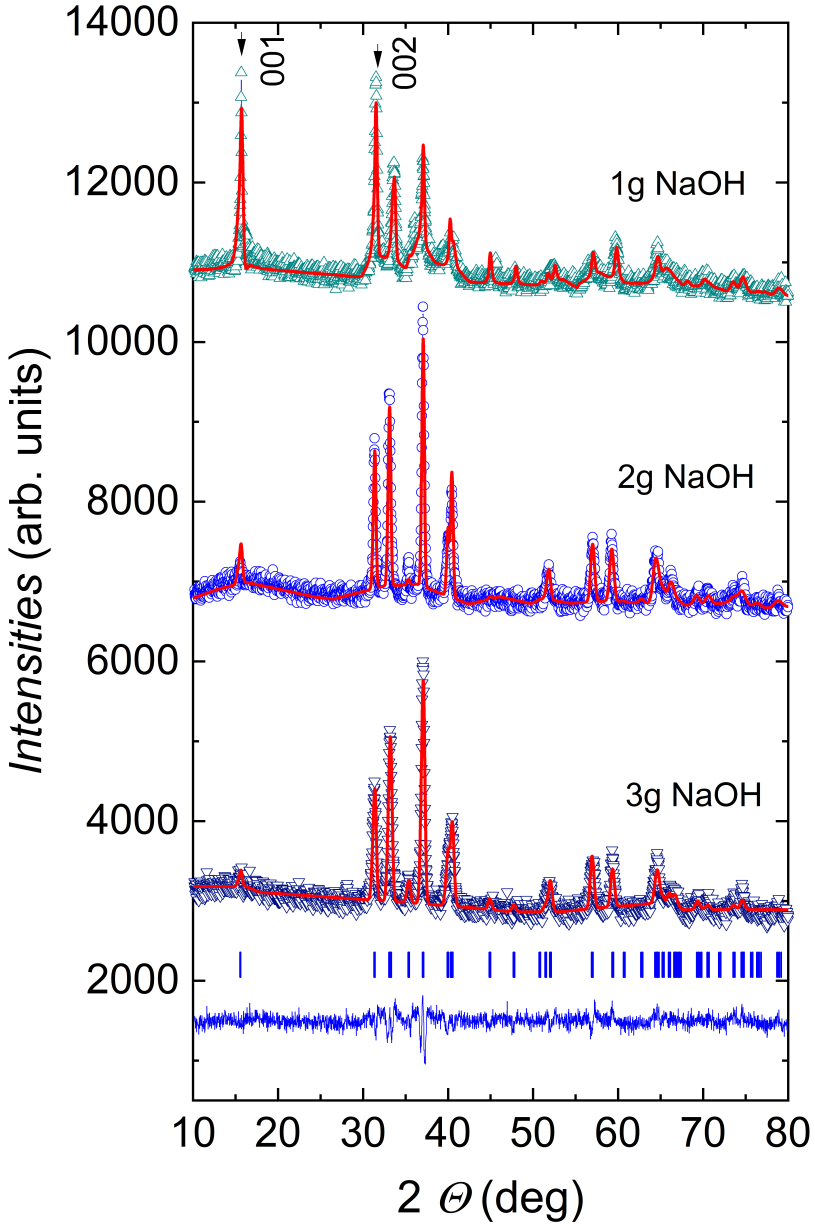

Figure 2: XRD patterns of the $CuMnO_2$ nanostructures synthesized by using different amounts of NaOH. The experimental data are denoted by open symbols, while the theoretical profiles by solid lines. The vertical scores spell the positions of Bragg reflections indexed in the C2/m space group. The line in the bottom is the difference between the experimental and theoretical data.

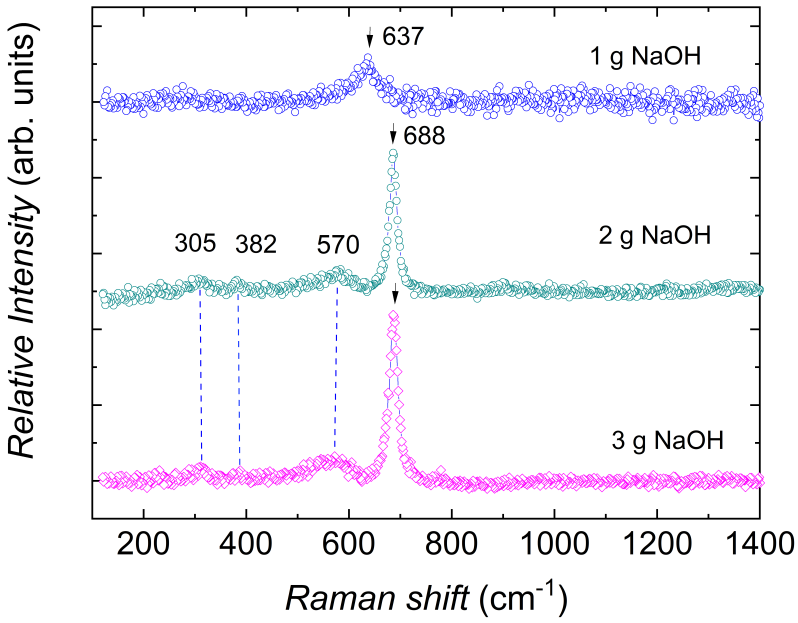

Figure 3: Raman scattering spectrum of the nanostructured $CuMnO_2$ synthesized by using different amounts of NaOH.

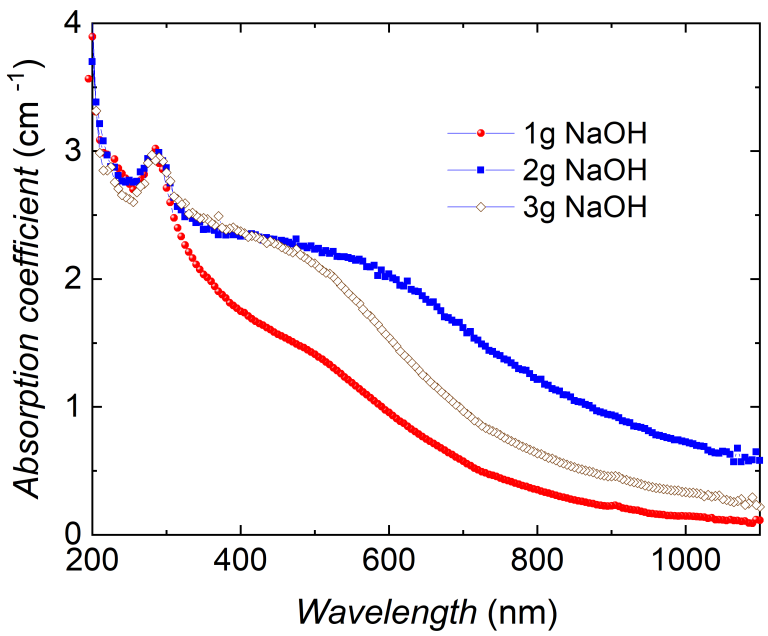

Figure 4: Absorption spectrum of the nanostructured $CuMnO_2$ synthesized by using different amounts of NaOH.

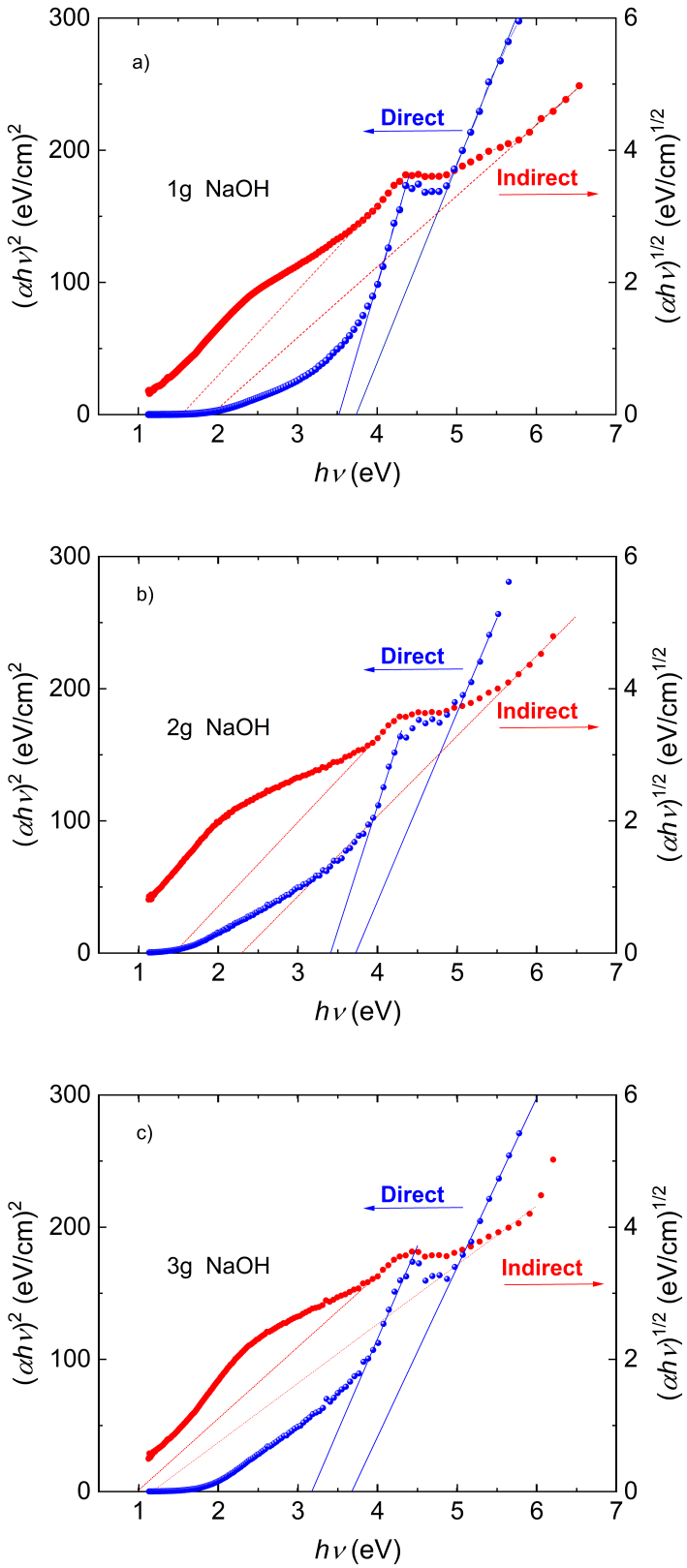

Figure 5: Experimental UV-VIS data (points) and Tauc law fittings (solid and dotted lines) for nanostructured $CuMnO_2$ samples synthesized by using different amounts of NaOH

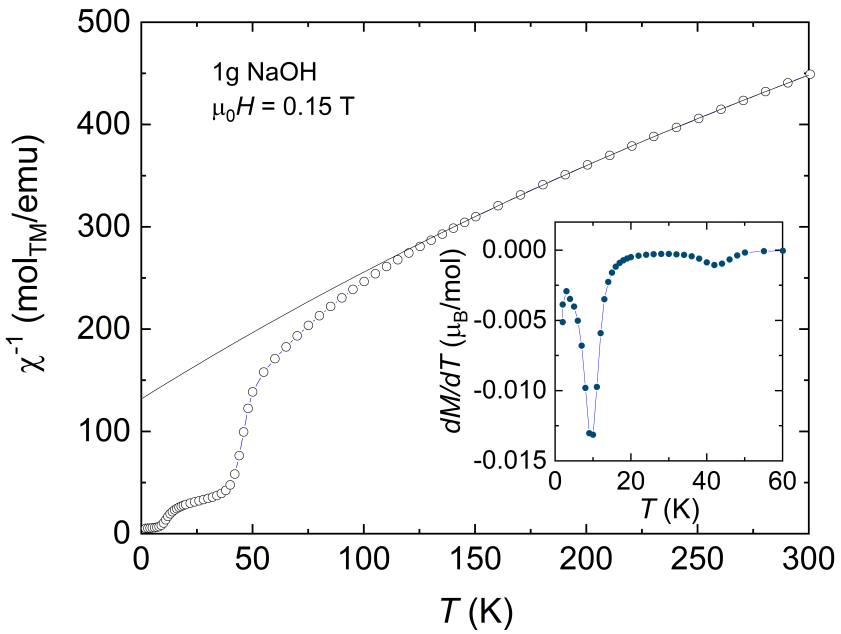

Figure 6: Temperature dependence of the inverse magnetic susceptibility of nanostructured $CuMnO_2$ obtained by using 1g NaOH. The solid line is a modified Curie-Weiss fit. The inset presents the temperature derivative of the magnetization.

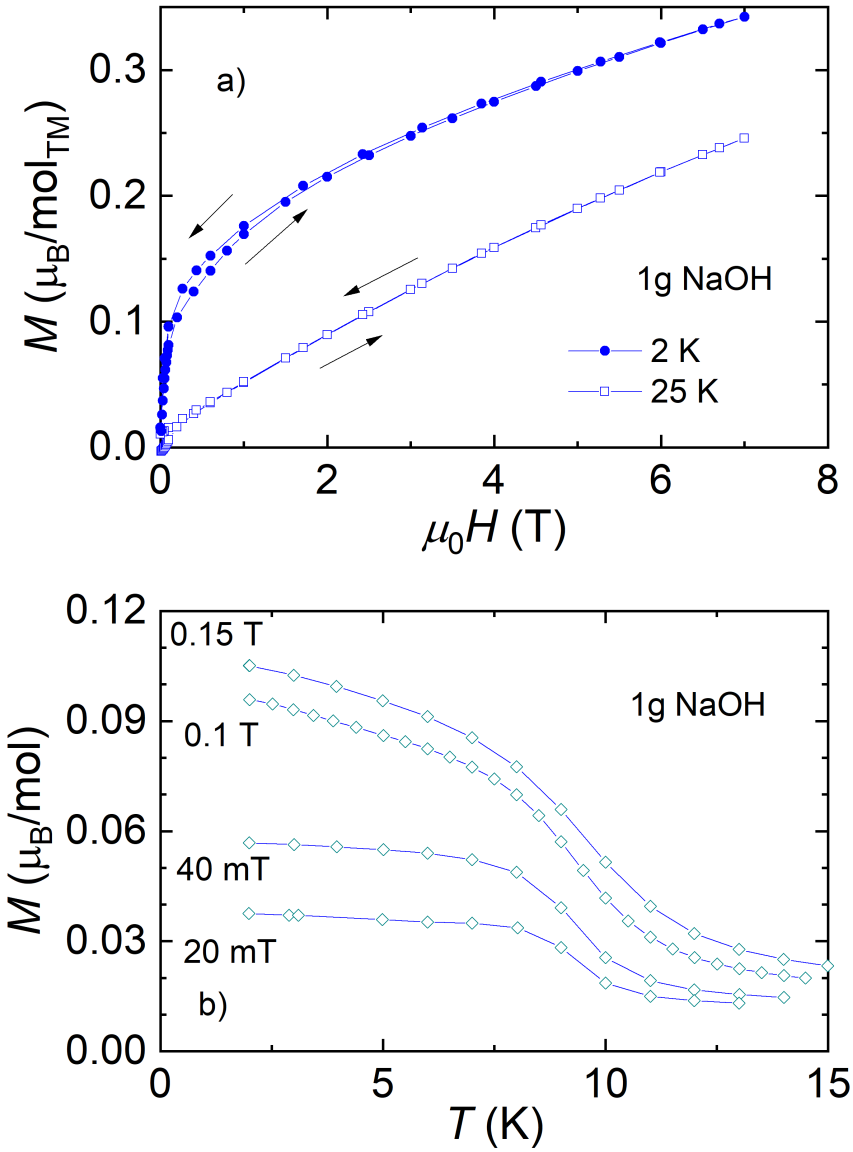

Figure 7: a) The magnetization collected at 2 and 25 K as a function of applied magnetic strengths and b) Temperature dependence of selected magnetization curves of nanostructured $CuMnO_2$ obtained by using 1g NaOH.

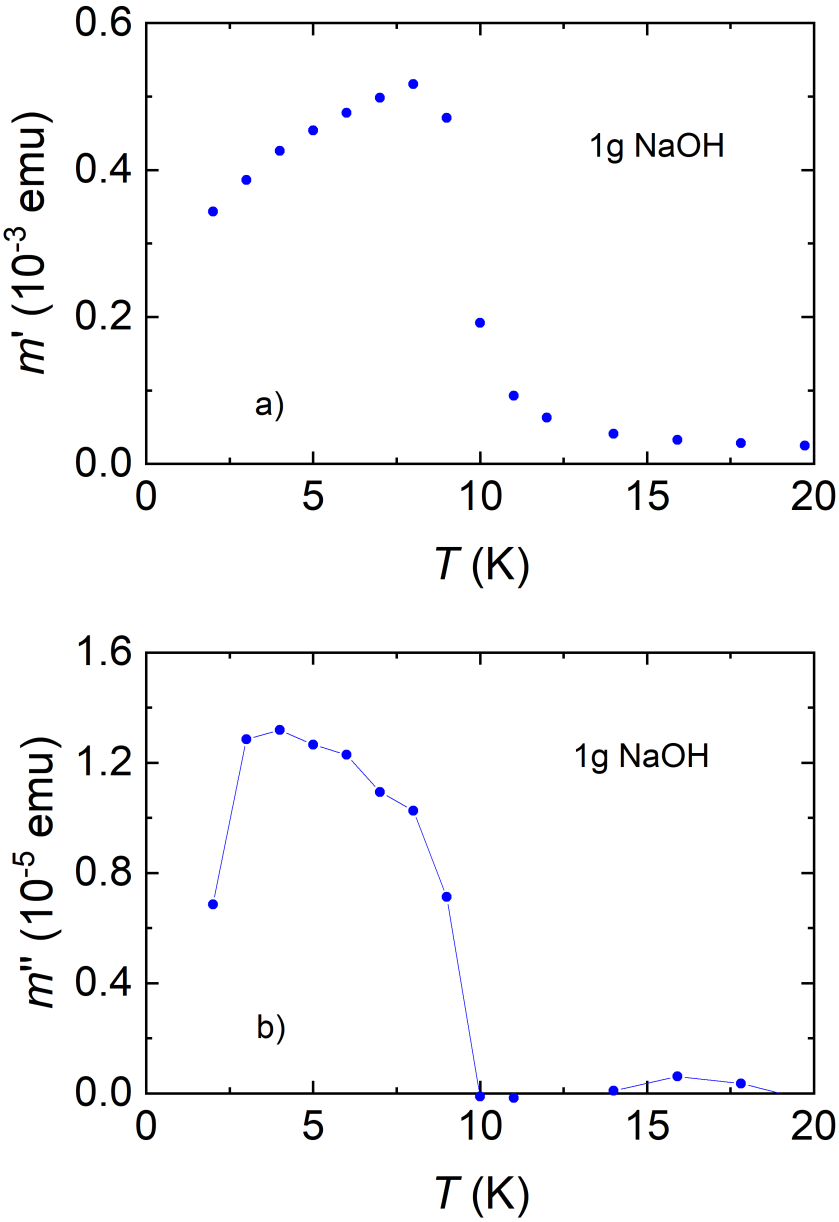

Figure 8: a) Temperature dependence of a) the real part and b) imaginary part of ac-magnetic susceptibility of nanostructured $CuMnO_2$ obtained by using 1g NaOH, measured with H_{ac} = 3 Oe and f = 1500 Hz.

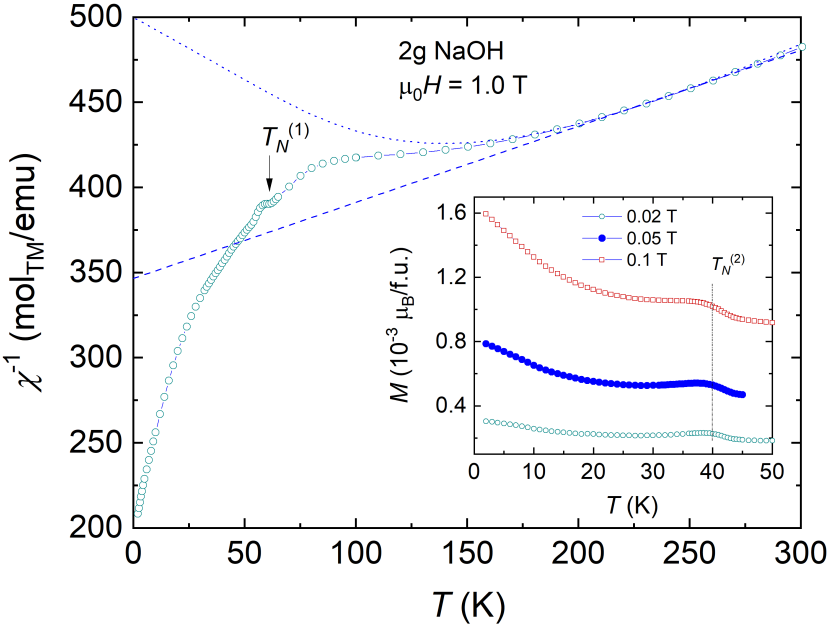

Figure 9: Temperature dependence of the inverse magnetic susceptibility of nanostructured $CuMnO_2$ obtained by using 2g NaOH. The dashed line is a fit of modified Curie-Weiss law and the dotted is S =5/2 Heisenberg model fit to the experimental data. The inset depicts the magnetization collected in several fields versus temperature.

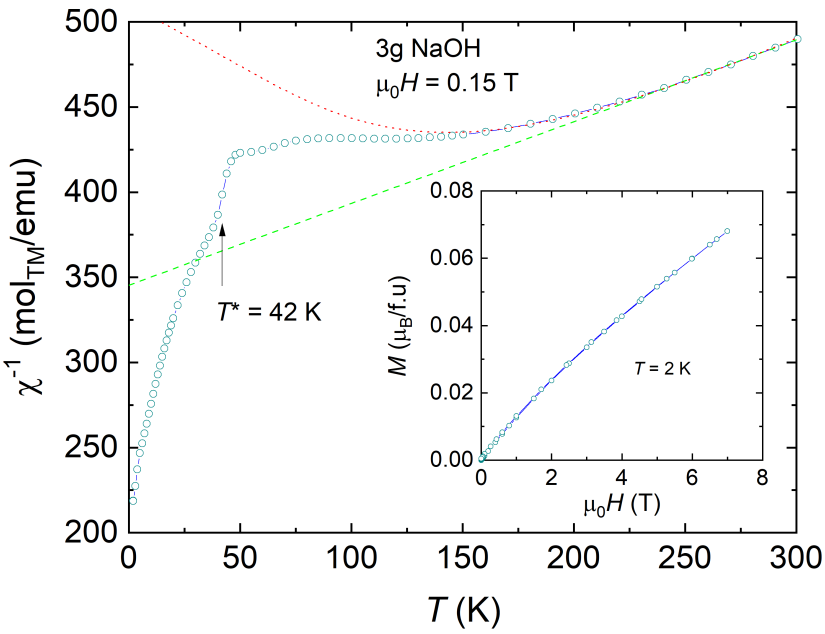

Figure 10: Temperature dependence of the inverse magnetic susceptibility of nanostructured $CuMnO_2$ obtained by using 3g NaOH. The dashed line is a fit of modified Curie-Weiss law and the dotted is S = 5/2 Heisenberg model fit to the experimental data. The inset depicts magnetization collected at 2 as a function of applied magnetic strengths.